THE ASTROPHYSICAL JOURNAL, 401:206–219, 1992 December 10

TWO-TEMPERATURE MODELS OF OLD SUPERNOVA REMNANTS WITH ION AND ELECTRON THERMAL CONDUCTION

WEI CUI AND DONALD P. COX
Department of Physics, University of Wisconsin-Madison, 1150 University Avenue, Madison, WI 53706
Received 1992 February 3; accepted 1992 June 17

ABSTRACT

To investigate the potential effects thermal conduction may have on the evolution of old supernova remnants, we present the results of one-dimensional (spherically symmetric) numerical simulations of a remnant in a homogeneous interstellar medium for four different cases: (1) without thermal conduction; (2) with both electron and ion thermal conduction assuming equal temperatures; (3) with electron thermal conduction only, following electron and ion temperatures separately; and (4) with both electron and ion thermal conduction following separate temperatures. We followed the entire evolution until the completion of the remnant bubble collapse. Some effects of magnetic field were considered, and comparisons with analytic results are made.

Our most significant result is that in remnant evolution studies concerned principally with either the shell or bubble evolution at late times, reasonable results are obtained with single-temperature models (such as those of Slavin and Cox who have been reevaluating the supernova bubble contribution to the interstellar porosity). When the electron and ion temperatures are followed separately, however, ion thermal conduction cannot safely be ignored.

Subject headings: conduction — ISM: bubbles — supernova remnants

1. INTRODUCTION

The importance of thermal conduction to the evolution of supernova remnants (SNRs) has been studied extensively for many years (e.g., Solinger, Rappaport, & Buff 1975; Chevalier 1975; Cowie 1977; Cox & Edgar 1983; Edgar & Cox 1984). Although conduction redistributes energy within the material, it has only second-order effects on the pressure distribution and therefore causes little change in the gross dynamics and evolution of growing remnants. However, thermal conduction markedly changes the adiabatic constant distribution in the remnant interior, and therefore the density structure there. At late times, when the SNR bubble is cooling and collapsing, the rate of cooling depends directly on that density structure and therefore on the entire previous history of thermal conduction.

Various attempts have been made to include thermal conduction in remnant evolution at various levels of approximation. Computer simulations include conduction in a single-temperature medium (Cioffi, McKee, & Bertschinger 1988; Slavin & Cox 1992), in a two-fluid approximation with separate electron and ion temperatures (but considering only electron thermal conduction) (Cowie 1977), and now with this paper, two fluids with separate electron and ion thermal conduction rates. Our goal is to learn what the details of this more complete calculation are, and over what periods of evolution one can confidently use results from the much simpler one-temperature model. Because this simpler model is being used extensively at the present time in various studies of remnant evolution, interstellar medium (ISM) porosity evaluation, local bubble formation, origin of the soft X-ray background and superbubble evolution, it is essential to know the reliability of this approximation.

In this study, the effects of thermal conduction on the structure and evolution of SNRs are limited to those found in one-dimensional hydrodynamic models of point explosions in a uniform medium.

We present the results for four calculations (summarized in Table 1) which begin with Sedov blast wave structures and include a useful approximation proposed by Kahn (1975) to the radiative cooling coefficient. The first case has no thermal conduction, but follows the electron and ion temperatures separately; the second includes thermal conduction under the assumption that the electron and ion temperatures are equal; the third follows electron and ion temperatures separately, with conduction limited to electrons; the fourth is like the third but includes the much slower ion thermal conduction as well. In all but the second case, it was assumed that electrons are not heated directly by the shock, so that only Coulomb collisions drive the electron temperature, T_e, toward the ion temperature, T_i. The particularly attractive feature of the Kahn cooling coefficient, $L = \alpha T_e^{-1/2}$, is that it yields a cooling time which, for otherwise adiabatic flow, is independent of a parcel's post-shock history, making possible the useful comparison with analytic results.

Previous studies (e.g., Cox 1972; Cox & Anderson 1982, and references therein) have shown that there are three distinct thermal periods in the evolution of a blast wave.

In the earlier period, Coulomb collisions are ineffective. If electrons are not heated by the shock, they remain rather cold. An analytical analysis presented by Itoh (1978, 1979) has been elaborated in subsequent work (references above). If, on the other hand, electrons were heated by the shock, then thermal conduction would be very rapid. As a limiting case, one might expect fast electron thermal conduction to lead to isothermal electrons while the much slower ion thermal conduction might leave the ions nearly adiabatic. A similarity solution for this case is presented in Cox & Edgar (1983). As we shall see below, however, the effects of ion thermal conduction are not negligible.

A second phase begins when Coulomb collisions eventually become able to force rapid equilibration between T_e and T_i in

TABLE 1

SUMMARY OF RESULTS

	Thermal Equilibration Mechanisms				
		Local		Global (Thermal Conduction)	
Case	$T_e = T_i$	Coulomb Collision	Shock Heating	Electron	Ion
1		•			
2	•		•	•	•
3		•		•	
4		•		•	•

the postshock gas. At about this same period, however, the potential conductive flux is falling rapidly compared to convective transport. The evolution toward equal temperatures is thus coeval with a return toward adiabaticity. Well before the onset of significant radiative cooling, the distribution of conditions behind the shock again approaches that of a Sedov (adiabatic) blast wave structure. The electron and ion temperatures are equilibrated, and thermal conduction is negligible. This return to an adiabatic evolution in the postshock region implies that earlier complications do not affect the later onset of radiative cooling.

The third phase, in which radiative cooling becomes important in the outer parts of the remnant, leads to the formation of a dense cool shell bounding a hotter diffuse bubble in the interior of the remnant. The outer boundary of the shell is a radiative shock. The inner boundary is a region of cooling and condensation flow from the bubble. (This sometimes leads to a transient inward facing radiative shock on the shell inner boundary.)

Conjectures on the subsequent evolution of the dense shell and hot bubble have been advanced for some time (e.g., Cox 1972; Cox & Smith 1974), but the situation was recently clarified by Slavin (1990), and Slavin & Cox (1992). The presence of nonthermal interstellar pressure and background heating of the gas leads to a weakening of the outer radiative shock and a reexpansion of the shell as its ram pressure drops toward ambient. The last vestige of the explosion is the slowly cooling bubble of hot gas. In addition, although thermal conduction is not important at this late stage, the existence of thermal conduction during the early evolution of the remnant substantially alters the distribution of density and temperature within the bubble at late times and has an enormous impact on its late-time history.

The present paper elaborates on this result, clarifying details and testing the effects of assumptions about the early thermal history. Slavin's (1990) work assumed a single temperature for both electrons and ions. We shall show that this does not harm his conclusions, our case 2 is like his, while our case 4 with all its complications leads to only slightly different behavior at all moderate to late times.

2. THE MODEL

We are modeling an isolated, spherically symmetric supernova remnant in a homogeneous interstellar medium, following the electron and ion temperatures separately. Several reasons why these temperatures may be different have been discussed in the literature referenced above. The principal reason is that the energy ahead of a stationary shock resides in the incoming ion kinetic energy; unless collisionless processes in the shock are effective in heating the electrons, electrons and ions achieve the same thermal speeds via deflection, i.e., $T_e = (m_e/m_i)T_i$ (Shklovskii 1973), where m_e is the mass of electron and m_i is that of ion. Thus thermalization of the incoming kinetic energy heats only the ions appreciably. Although the time scales are fairly short for achieving separate Maxwellian velocity distributions for the ions and electrons, the time scale for equilibration of their two temperatures is not negligible. In addition, the two species have different transport and emission rates.

The basic hydrodynamical equations employed can be written as follows:

$$\frac{D\rho}{Dt} = -\frac{\rho}{r^2}\frac{\partial}{\partial r}(r^2 v) \tag{1}$$

$$\rho\frac{Dv}{Dt} = -\frac{\partial}{\partial r}\left(P_{\rm th} + \frac{B^2}{8\pi}\right) \tag{2}$$

$$\frac{D}{Dt}\left(\frac{P_{\rm th}}{\rho^\gamma}\right) = -\frac{\gamma - 1}{\rho^\gamma}\left[\frac{1}{r^2}\frac{\partial}{\partial r}(r^2 F) + L n_e^2\right], \tag{3}$$

where $P_{\rm th}$ is thermal pressure, n_e is electron number density, γ is adiabatic index, $\gamma = \frac{5}{3}$, L is radiative cooling coefficient and F is total thermal conduction flux.

The magnetic pressure term is included here to idealize the effects that a magnetic field might have on the evolution of a SNR. This was discussed in great detail by Slavin & Cox (1992, hereafter SC). Here we simplify the problem in the same way, including only magnetic pressure in the momentum equation, and assuming that thermal conduction is unimpeded by the magnetic field. (The latter exaggerates the effects of thermal conduction to an as yet unknown degree.) The evolution of the magnetic field, B, is taken to follow $B = B_0(n/n_0)$ as in one-dimensional transverse field problems, where n is the density. Alternatives are discussed in SC.

We require an additional equation separating the evolution of electron and ion temperatures, a prescription for evaluating the electron and ion thermal conduction fluxes, and a radiative cooling coefficient, L.

Coulomb collisions in fully ionized gas have been studied extensively (Spitzer 1962); the volumetric energy transfer rate from ions to electrons is

$$h = a k_{\rm B} n^2 \frac{T_i - T_e}{T_e^{3/2}}, \tag{4}$$

where n is the number density of the gas, $k_{\rm B}$ is Boltzmann's constant, T_i is the ion temperature, T_e is the electron temperature and (Cox & Edgar 1983)

$$a \approx \frac{\ln\Lambda}{153}\ {\rm cgs}\ , \quad \ln\Lambda \approx \ln\left[1.2 \times 10^5\left(\frac{T^{1/2}T_e}{n^{1/2}}\right)\right]. \tag{5}$$

At early times, Coulomb collisions are too rare to force T_e to T_i, but become gradually more important. A plateau forms on the electron temperature distribution, with h effectively canceling adiabatic expansion losses. The ions gradually cool via both expansion and heating of the electrons until they reach the electron temperature.

The time scale to achieve $T_e = T_i$ near the shock front is (e.g., Itoh 1978)

$$t = 5000\ {\rm yr}\ E_{51}^{3/14} n_0^{-4/7}\ , \tag{6}$$

where E_{51} is the explosion energy in units of 10^{51} ergs, and n_0 is the ambient density.

We define an average temperature of the system

$$T = \frac{n_i T_i + n_e T_e}{n_i + n_e} \tag{7}$$

and an equilibration factor

$$g = \frac{T_e}{T}, \tag{8}$$

where n_i and n_e are the number densities of ions and electrons, respectively. Note that $n_i = n$.

After some mathematical manipulations in equation (4), we get

$$h = \chi \frac{a k_B n^2}{T^{1/2}} \frac{1-g}{g^{3/2}}. \tag{9}$$

Using the ideal gas law for both electron and ion pressures one can show that

$$p_i = p_{th}\left(1 - \frac{n_e}{n_e + n_i} g\right) \tag{10}$$

$$p_{th} = \chi n k_B T, \tag{11}$$

where p_i is the ion pressure, while p_{th} is the total gas pressure and $\chi \equiv (n_i + n_e)/n$.

Let ϵ be the effective volumetric "emissivity" of the system:

$$\epsilon = L n_e^2 + \nabla \cdot F_e + \nabla \cdot F_i, \tag{12}$$

where F_e is the heat flux of electron thermal conduction, and F_i is that of ion thermal conduction.

Of these terms, $L n_e^2 + \nabla \cdot F_e$ is the loss rate per unit volume taken from the electrons, while $\nabla \cdot F_i$ is that from the ions. The ions also have h as a loss term, while the electrons see it as a source. Separating the energy equation into total and ionic components, we have

$$\frac{D}{Dt}\left(\frac{p_i}{n^{5/3}}\right) = -\frac{3}{2}\frac{h + \nabla \cdot F_i}{n^{5/3}} \tag{13}$$

$$\frac{D\kappa}{Dt} = \frac{D}{Dt}\left(\frac{p_{th}}{n^{5/3}}\right) = -\frac{2}{3}\frac{\epsilon}{n^{5/3}}, \tag{14}$$

where we have introduced the adiabatic constant $\kappa \equiv p_{th}/n^{5/3}$. Combining these with equations (9) and (10), we get

$$\frac{Dg}{Dt} = \frac{2}{3}\frac{n}{n_e}\chi\left[a\left(\frac{\chi k_B}{\kappa}\right)^{3/2}\frac{1-g}{g^{3/2}} + \frac{\nabla \cdot F_i}{\kappa n^{5/3}} - \frac{\epsilon}{\kappa n^{5/3}}\left(1 - \frac{n_e g}{n\chi}\right)\right]. \tag{15}$$

To simplify numerical integration when g is small, it is convenient to introduce

$$f \equiv \frac{3}{2}\ln\left(\frac{1 + g^{1/2}}{1 - g^{1/2}}\right) - g^{1/2}(g + 3),$$

which by differentiation yields

$$\frac{Df}{Dt} = \frac{3}{2}\left(\frac{g^{3/2}}{1-g}\right)\frac{Dg}{Dt},$$

and therefore

$$\frac{Df}{Dt} = \frac{n}{n_e}\chi\left[a\left(\frac{\chi k_B}{\kappa}\right)^{3/2} + \frac{g^{3/2}}{1-g}\frac{\nabla \cdot F_i}{\kappa n^{5/3}} - \frac{\epsilon}{\kappa n^{5/3}}\frac{g^{3/2}}{1-g}\left(1 - \frac{n_e g}{n\chi}\right)\right]. \tag{16}$$

We follow the evolution of f for each parcel, inverting at each step to find the implied value of g. Cox & Anderson (1982) found a good approximation for the inversion to be

$$g(f) \approx 1 - \exp\{-(5/3f)^{2/5}[1 + 0.3(5/3f)^{2/5}]\}. \tag{17}$$

By integrating equation (16) and applying equation (17), along with integrating $D\kappa/Dt$, Dv/Dt, and $D\rho/Dt$, one finds p_{th} from $\kappa = p_{th}/n^{5/3}$, T from $p_{th} = \chi n k_B T$, and $T_e = gT$, successfully separating the equations.

Separating thermal conduction flux into electronic and ionic components is not as trivial as the approach we present below. For example, conduction is constrained to maintain approximate charge neutrality. This is enhanced by an electric field along ∇T. The presence of this field necessarily couples the transport rates of the two species.

Classical thermal conduction obeys $F_{class} = -\kappa_c \partial T/\partial r$. In fully ionized gas, κ_c for the electron system has been found (Spitzer 1962) $\kappa_{ce} = \beta_e T_e^{5/2}$, $\beta_e \approx 6.0 \times 10^{-7}$ cgs, and very similarly, for ion thermal conduction, we have $\kappa_{ci} = \beta_i T_i^{5/2}$, where Braginskii (1958) found $\beta_e/\beta_i \approx 27.65$, not $[(m_i/m_e)]^{1/2} \approx 48.3$ as expected from the ratio of average particle speeds. The cause is said to be that both electron-electron and electron-ion collisions impede electron thermal conduction, while, for ion thermal conduction, only ion-ion collisions are important. We would expect that there might also be a difference in the suppression factor imposed by charge neutrality, but have adopted the above results.

Thermal conduction saturates when the temperature changes significantly over a particle's effective mean free path (Cowie & McKee 1977). In this case, Cowie & McKee (1977) recommended an expression much like

$$F_{sat\,e} = 13.8\phi_s(n_e k_B T_e)\left(\frac{k_B T}{m}\right)^{1/2}, \tag{18}$$

where $\phi_s \approx 0.3$, except we have replaced T_e with T in the final bracket. Ion thermal conduction is much slower, mainly due to the much larger mass of the ions, just as in the classical conduction case. We assume that it is also a factor of 27.65 slower to find

$$F_{sat\,i} = 0.5\phi_s(n_i k_B T_i)\left(\frac{k_B T}{m}\right)^{1/2}. \tag{19}$$

To calculate the total heat flux, F, we use

$$\frac{1}{F} = \frac{1}{F_{sat}} + \frac{1}{F_{class}}, \tag{20}$$

to calculate F_i and F_e separately.

We do not claim that the above expressions are the correct ones, but they represent our present best guesses for the rates. Our only modification to the usual rates for electron conduction is due to the use of the average temperature T in the calculation of the characteristic speed. We think this is more appropriate in the context of the free molecular conductivity formalism used by Cowie & McKee (1977) to make the esti-

mate. The difference will be important in the application below only where the ions are significantly hotter than the electrons, and in such places the electron temperature distribution tends to be quite flat and far from saturation anyway. For the saturated ion conductivity, with equation (19) and $\phi_s = 0.3$, our rate is 1/16 of the product of the energy density and the mean speed. We expect this to be a lower limit to the saturated flux, with an upper limit about an order of magnitude larger. We have tried both values, and found the difference to be potentially important, as discussed in the results below.

For the radiative cooling coefficient, we have adopted an approximation proposed by Kahn (1975, 1976), $L \approx \alpha T_e^{-1/2}$, where $\alpha \approx 1.3 \times 10^{-19}$ cgs provides a reasonable fit to the Raymond, Cox, & Smith (1976) cooling curve for collisional equilibrium for $4 \times 10^5 \leq T_e \leq 5 \times 10^7$ K. This expression has the analytic advantage of being integrable when $T_e = T_i$ and $\nabla \cdot F = 0$:

$$\frac{D\kappa}{Dt} = -\frac{2}{3}\frac{Ln^2}{n^{5/3}} = -\frac{2}{3}\frac{\alpha n^{1/3}}{T^{1/2}} = -\frac{2}{3}\frac{\alpha n^{5/6}}{(p_{\rm th}/\chi k_{\rm B})^{1/2}} = -\frac{2}{3}\alpha\frac{(\chi k_{\rm B})^{1/2}}{\kappa^{1/2}} \quad (21)$$

$$\kappa^{3/2} = \kappa_0^{3/2} - \alpha(\chi k_{\rm B})^{1/2}(t - t_0)\,, \quad (22)$$

where t_0 is the time when the parcel was shocked, and κ_0 is the adiabatic constant of the parcel at $t = t_0$. Thus the residual cooling time from adiabat κ is always

$$\Delta t_{\rm cool} = \frac{\kappa^{3/2}}{\alpha(\chi k_{\rm B})^{1/2}} = \frac{p_{\rm th}}{Ln^2}\,. \quad (23)$$

This result will be extremely useful in interpreting model results presented below.

The numerical method used in this paper is described in detail in SC, except for our use of Kahn's cooling formula and our separation of electron and ion temperatures. Rather than starting from the very beginning of the explosion, waiting for the structure to relax, we have initialized with the Sedov solution at a radius of 2 pc when the enclosed mass is approximately 1 $M_\odot$.

Equations (16) and (17) are the theoretical basis for our electron temperature routine. We have adopted a single step, forward time finite difference scheme to solve equation (16) numerically.

It is assumed that the explosion occurs in a homogeneous medium with density $n_0 = 1$ cm^{-3}, magnetic field $B_0 = 5.0$ μG, ambient temperature $T_0 = 10^4$ K, and the explosion energy $E_0 = 0.5 \times 10^{51}$ ergs. Also, $n_i = n_{\rm H} + n_{\rm He}$, where $n_{\rm H}$ is the number density of hydrogen atoms, and $n_{\rm He}$ is that of helium atoms, assuming $n_{\rm He} = 0.1 n_{\rm H}$. Cooling was assumed to follow

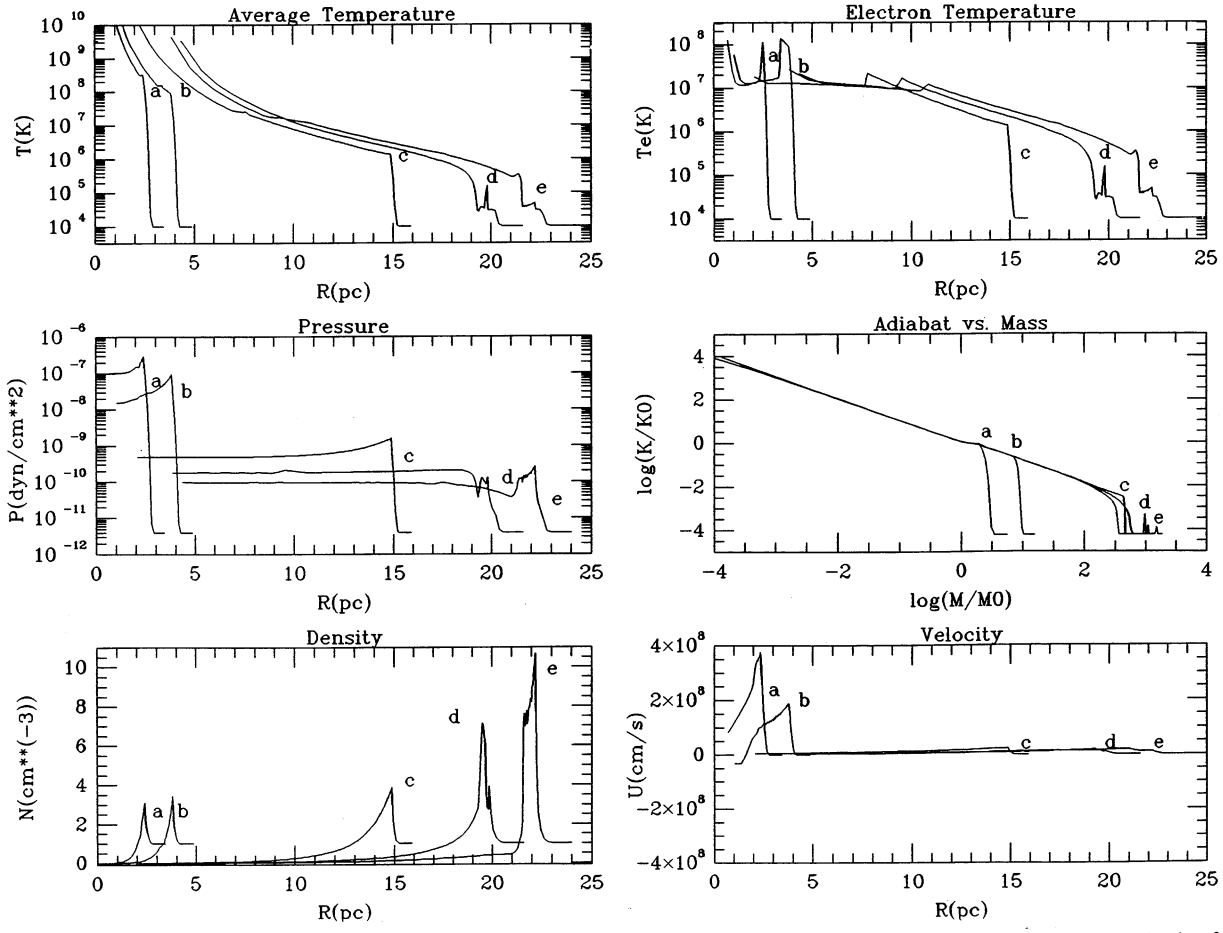

FIG. 1.—Average temperature, electron temperature, total pressure, adiabat, density, and velocity distributions of the SNR for case 1 (conduction-free) at times (curve a) 200, (curve b) 600, (curve c) 18,000, (curve d) 40,000, and (curve e) 60,000 yr after the explosion.

the Kahn approximation down to T_0, at which point L was set equal to 0.

We have used 200 parcels in the program. Initially the spacing between adjacent parcels is 0.1 pc, and there are 20 parcels within the shock. As the shock propagates outward, more parcels get swept up; as soon as the shock front gets to the 200th parcel, we rezone by doubling the spacing between parcels.

3. NUMERICAL RESULTS

3.1. *Case 1*

In this case, thermal conduction is neglected. At early stages (curves a, b, and even c in Figure 1), radiative cooling has not yet become important, and the SNR evolves adiabatically. The structure continues to be very well described by the Sedov similarity solution as expected. In this phase, there are two constants of motion associated with a parcel, its adiabatic constant, κ, and total mass of matter interior to it, M. The inverse proportionality expected between these two is verified in the adiabatic constant distribution plot. At around 40,000 years, parcels just interior to the shock cool off (see curves d and e in Fig. 1). The SNR then deviates from the Sedov-like structure. Near the shock front, a dense shell forms around a hot, low-density region, the so-called bubble. This hot center, however, still evolves nearly adiabatically though cooling eats into it from the outside as is apparent from the evolution of the adiabatic distribution.

A comparison of the electron and average temperature distribution plots clearly shows the nonequilibration zone in the remnant center where $T_i > T_e$ (see curves c, d, and e in Fig. 1).

As the evolution continues, the shock becomes weaker and less compressive, the pressure more nearly constant in the central region. The hot bubble continues expanding; the shell becomes thicker and less dense. At around 600,000 yr, the bubble starts to collapse. Figure 2 shows the structure at late times. The hot bubble shrinks very slowly as it cools off, roughly in pressure balance with the surroundings.

3.2. *Case 2*

Now we include thermal conduction, but assume $T_i = T_e$ due to shock heating of electrons and other unspecified but required mechanisms. The structure is initialized with a Sedov-like solution, but evolves rapidly to a non-Sedov structure. As we can see in Figure 3, the temperature profile is flattened by thermal conduction, starting from the hot central region, but gradually expanding outward. Cooling sets in around the same time as in case 1 followed by similar shell formation and bubble isolation.

The adiabatic constant distribution evolves to a structure very different from that of case 1. In the central region it is

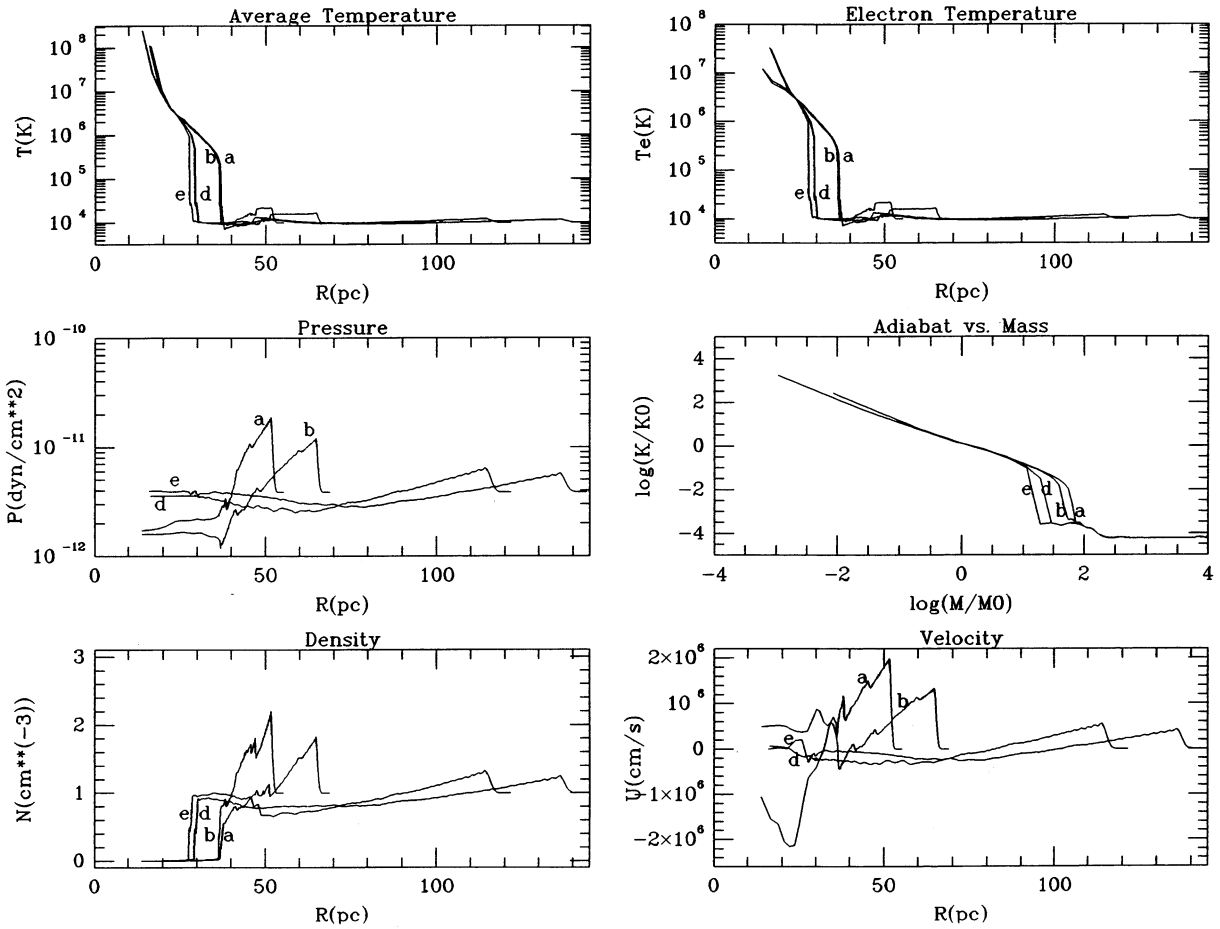

FIG. 2.—Same kind of distributions as those in Fig. 1 at times (curve a) 6×10^5, (curve b) 10^6, (curve d) 3×10^6, and (curve e) 4×10^6 yr after the explosion, this is the collapsing phase of the hot bubble.

much more nearly isentropic. At late times, the fact that the adiabatic distribution in the remnant center is very nearly independent of time shows that conduction has practically stopped. Nevertheless the effects of its earlier activity are still very significant. When the hot bubble stars to collapse (Fig. 4), the temperature profile is fully flattened making the density and cooling rate within the bubble much higher than in the corresponding conduction-free case. At around 3 million years, the hot bubble completes its cooling and merges with ambient ISM.

3.3. *Case 3*

Here we ignore ion thermal conduction, but include electron thermal conduction, as was done traditionally, while treating electron and ion temperatures separately. The structure of this two-temperature system is surprisingly similar to that in case 1 for the hot central region where $T_i > T_e$, but changes abruptly to resemble case 2 outside that nonequilibrated region (Fig. 5). Looking at temperature profiles, we see extreme segregation of the hot ion zone where the electron temperature is flattened by its thermal conduction, but Coulomb collisions are not sufficient to equilibrate electrons and ions. (The structure is never like the similarity solution of Cox & Edgar (1983), because we do not assume shock heating of electrons.)

The very hot ions in the central region keep some energy away from the equilibrated zone. This has little effect on the overall structure for $t \leq 10^5$ yr, making it very similar to case 2; later, however, it gradually begins to resemble case 1 as the slowly equilibrating core releases energy into the bubble (Fig. 6).

3.4. *Case 4*

Here we have extended case 3 by including ion thermal conduction with the saturation limit as in equation (19). We see a rapid flattening of the ion temperature profile (Fig. 7) which enhances the coupling of electron and ion temperatures, but not enough to eliminate the hot ion core entirely. The structure outside that zone is very similar to case 2. The late evolution shown in Figure 8 is close to that in Figure 4, except very near the end of the bubble lifetime when the energy in the hot ion core is still being released, extending the lifetime in this case.

When this case is repeated with a factor of 10 larger saturated ion flux, the results are essentially indistinguishable from case 2. The hot ion core quickly disappears entirely and there is no other important distinction. This similarity continues throughout the bubble collapse period, including the bubbles having the same time for their final disappearance.

We conclude that the magnitude of the saturation limits for the ion flux does make some difference to the structure, and that case 4 represents the minimal inclusion of ion thermal conduction.

4. COMPARISON OF BUBBLE EVOLUTIONS

A major goal for studies of this type is to evaluate the late-time evolution of SNR bubbles sufficiently well that we can begin to make useful estimates of the porosity of the interstellar medium (Cox & Smith 1974; McKee & Ostriker 1977; SC 1992; Cox & Slavin 1992). In Figure 9 we show the time histories of the shock and bubble radii for the four cases above. The shell is that region between these two radii and is a rather meaningless concept after about 10^6 yr.

The shock evolution is completely insensitive to the conduction parameters (e.g., Solinger et al. 1975; Chevalier 1975; Cowie 1975), while bubble evolution is critically sensitive. Case 3, with electron but not ion conduction, is physically unrealiz-

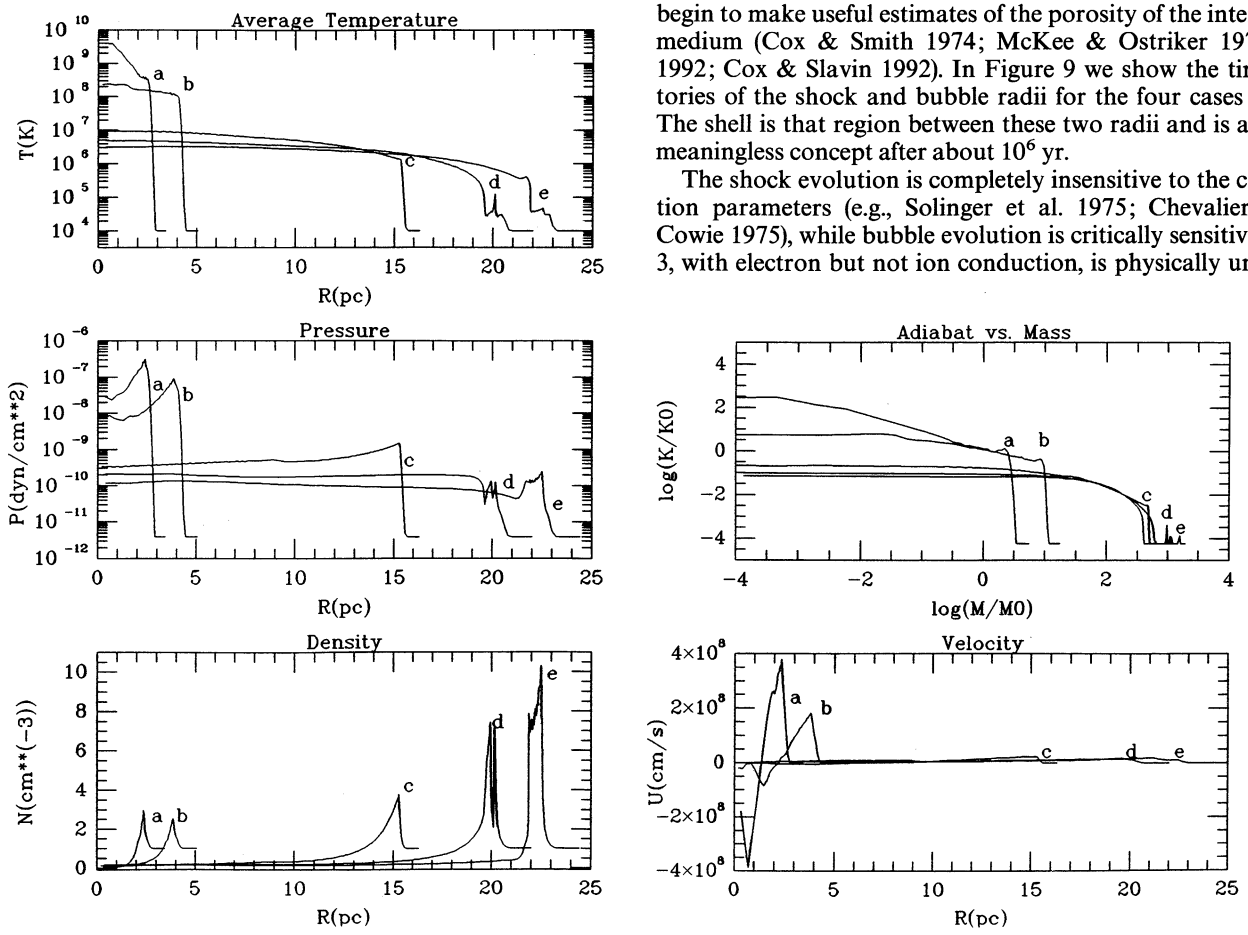

FIG. 3.—Same distributions as those in Fig. 1, but for case 2 (including both electron and ion thermal conductions, but assuming $T_i = T_e$), only the average temperature distribution is shown since the electron temperature distribution is the same.

able, and we will not discuss it further. Among the remaining cases, 2 and 4 are much more alike than either is to case 1. In addition, a higher ion saturated flux would make 4 even more like 2. As a consequence, the late time evolution depends much more on whether or not conduction occurs (case 1 vs. 2) than whether there are processes to enforce $T_e = T_i$ (case 2 vs. 4).

It is obvious that this one remaining worry is a major one. The porosity estimates depend on $\int V_B\,dt$ where V_B is the bubble volume. If thermal conduction is completely suppressed by an unfavorable magnetic field configuration, the insulated hot bubble takes an enormous time to cool. Conversely, if conduction was active before the shell formation epoch, the bubble has a higher density and lower temperature at late times, and radiates rather rapidly.

This point is amplified and put into a better context by Figure 10 which shows the amount of mass hotter than 10^5 K as a function of time for cases 1, 2, and 4. Without conduction, parcel adiabats drop only by radiation. We shall show below that the Sedov distribution of adiabats at early time plus Kahn cooling are sufficient to predict the case 1 hot mass versus time curve of Figure 10. Case 2 with conduction, however, has roughly 50 $M_\odot$ more material inside its bubble, mainly near the center where case 1 has an extremely low density. This last 50 $M_\odot$ has nearly constant adiabat and therefore nearly identical cooling time. The bubble cools precipitously after this plateau adiabat is reached, hence the sudden cooling of this case in Figure 10.

A sobering feature of Figure 10 is that at $t \approx 2.5 \times 10^6$ yr, when case 2 is finishing its evolution, the roughly 30 pc radius bubble of case 1 contains less than 20 $M_\odot$. Thus, the late evolution of bubbles also depends sensitively on the adiabat distribution created during the very early stage of remnant evolution, including effects due to clumping, mixing of ejecta, and so on.

Case 4, with minimal ion conduction, shows a bubble mass track very similar to case 2 prior to 10^6 yr. Thereafter, the energy in the hot ion core stretches the lifetime by 0.6 million yr. This difference disappears entirely if case 4 has the larger ion saturated flux discussed previously.

5. ANALYTIC COMPARISONS

The principal features of these evolutions and the differences between them can be confirmed by analytic approximations.

5.1. *The Hot Ion Zone*

In cases 1,3, and 4, the unequilibrated zone is very prominent. It plays a major role in the evolution of case 3, a modest role in case 4. Following Cox & Anderson (1982, who follow Itoh), one finds that at the equilibration boundary ($T_e = T_i$), the adiabatic constant obeys

$$\kappa_{eb} = \chi k_B \left(\frac{5}{3}\frac{\ln\Lambda}{81}\,t\right)^{2/3}. \tag{24}$$

In case 1, the distribution of adiabats within the hot bubble is just that provided by the Sedov evolution. As a function of enclosed mass it is

$$\kappa(M) = \frac{p_s(M)}{(4n_0)^{5/3}} = \frac{2.025\pi m E_0}{25(4n_0)^{2/3}M} \tag{25}$$

where $m = \rho/n$. Because the pressure within a hot bubble is nearly uniform, the distribution of adiabats provides the dis-

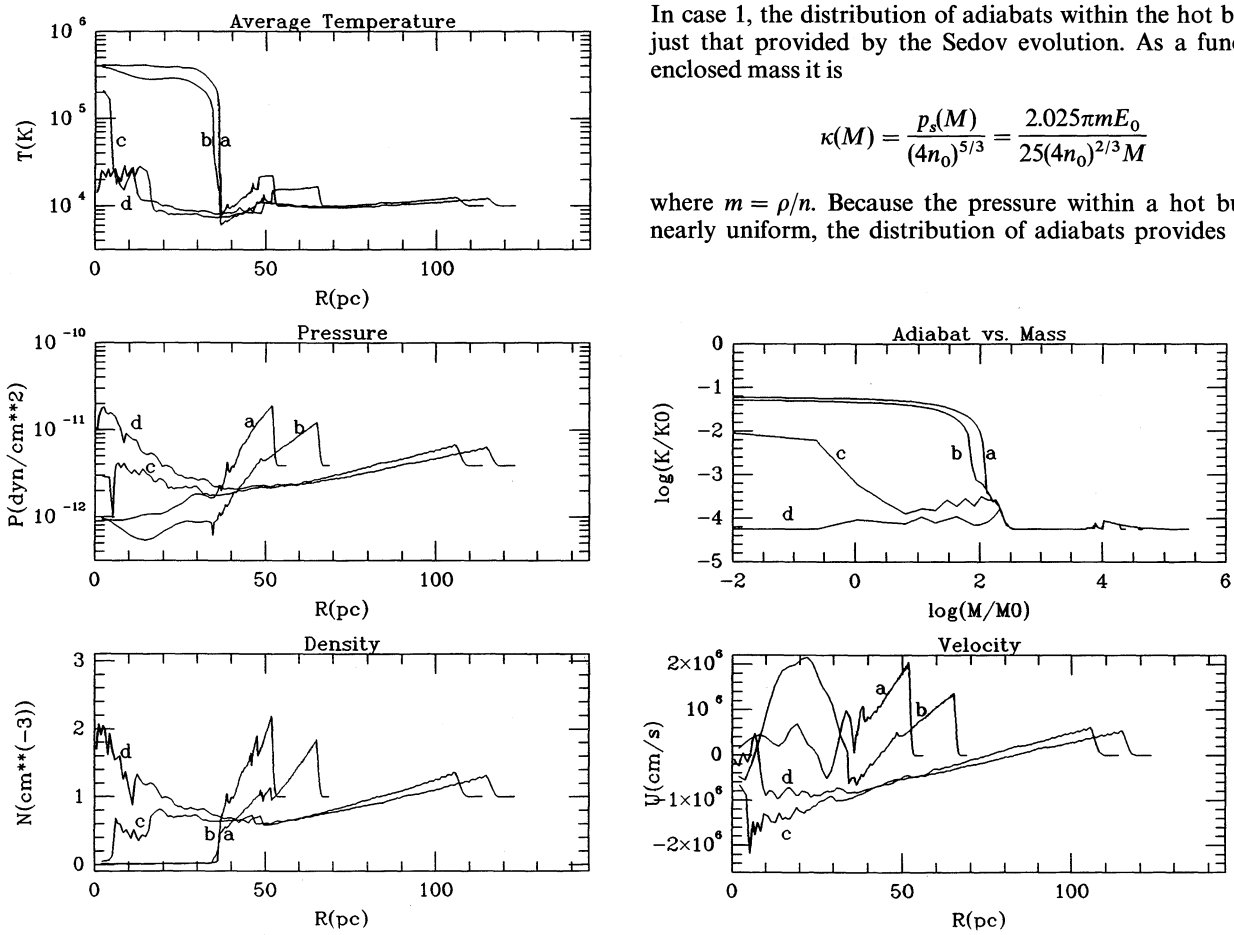

FIG. 4.—Same kind of distributions as those in Fig. 3 at times (curve a) 6×10^5, (curve b) 10^6, (curve c) 2.6×10^6, (curve d) 3×10^6 yr, collapsing phase of the hot bubble.

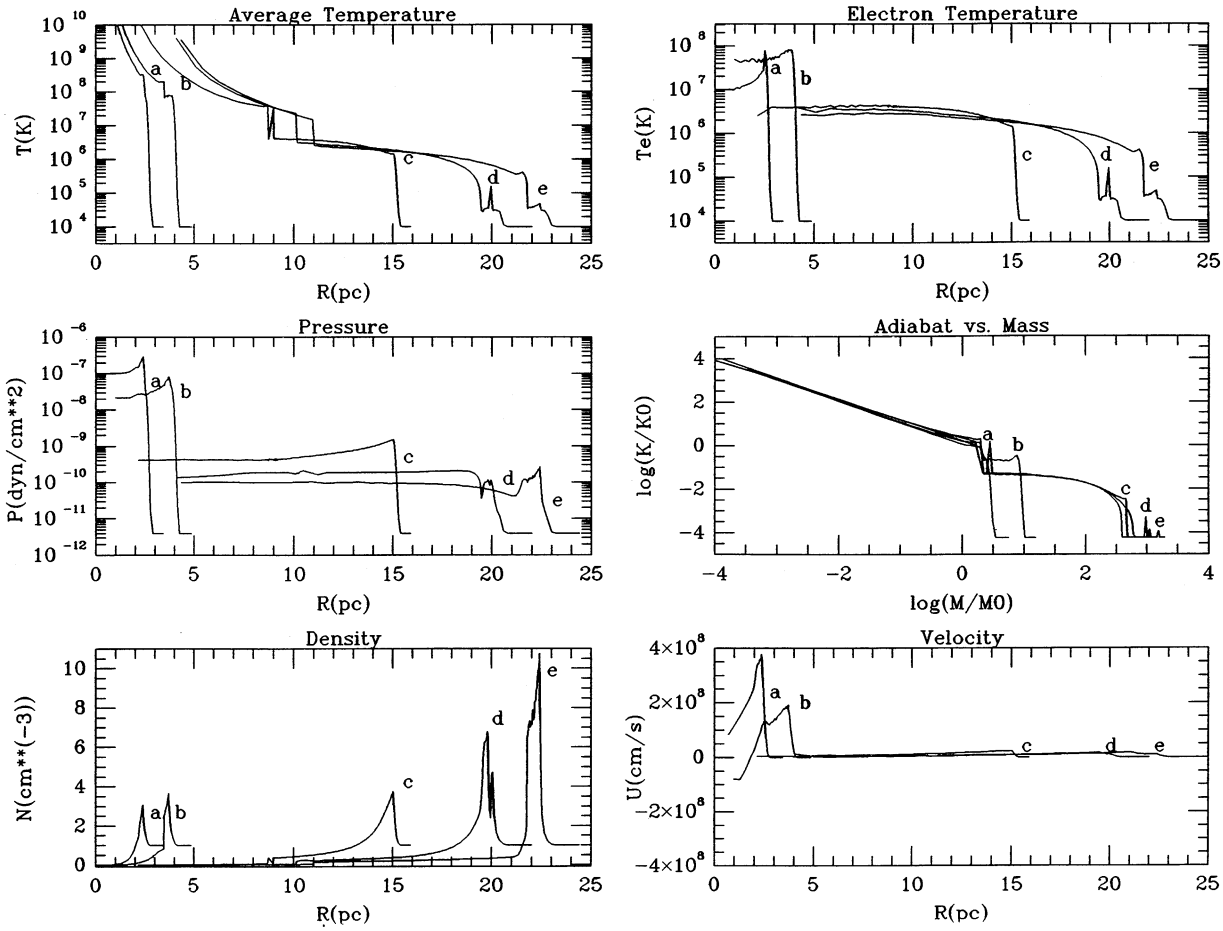

FIG. 5.—Same distributions as those in Fig. 1, but for case 3 (only electron thermal conduction is included)

tribution of density:

$$\frac{dM}{dV} = mn = m\left[\frac{p}{\kappa(M)}\right]^{3/5} . \tag{26}$$

For $\kappa M = \kappa_1 M_1$ constant as above, this distribution yields

$$V = \frac{5}{2m}\left(\frac{M_1\kappa_1}{p}\right)^{3/5} M^{2/5} = \frac{5}{2m}\frac{M_1\kappa_1}{p^{3/5}\kappa^{2/5}} . \tag{27}$$

Taking κ_{eb} from equation (24) and $\kappa(M)$ from equation (25), the radius of the hot ion zone should be

$$R_{eb} \approx 20 \text{ pc} \frac{(2E_{51})^{1/3}}{t_{myr}^{4/45}} \frac{1}{n_0^{2/9}} \left(\frac{10^{-12}}{p_{center}}\right)^{1/5} . \tag{28}$$

In Figure 1, curve c we find $p_{center} \approx 5 \times 10^{-10}$ dyn cm^{-2}, $t \approx 2 \times 10^4$ yr, thus our predicted value for R_{eb} is then 8.1 pc, in good agreement with the roughly 7.7 pc found on the figure.

5.2. *The Shell Formation Epoch*

Again following Cox & Anderson (1982) who follow Kahn, the first parcel to cool enters the shock at time

$$t_1 \approx 3 \times 10^4 \text{ yr} \frac{(E_{51})^{3/14}}{n_0^{4/7}} \tag{29}$$

when the radius is

$$R_1 \approx 16 \text{ pc} \frac{(2E_{51})^{2/7}}{n_0^{3/7}} \tag{30}$$

and the enclosed mass

$$M_1 = 545\ M_\odot \frac{(2E_{51})^{6/7}}{n_0^{2/7}} . \tag{31}$$

It finishes cooling, marking the shell formation epoch at $t_{cool} = (14/9)t_1$, for our case at 4×10^4 yr, in excellent agreement with the numerical simulations.

5.3. *Bubble Mass and Radius Evolution (No Thermal Conduction)*

Use of Kahn's approximation to the cooling function makes it easy to find a reliable approximation to the mass within the hot bubble at late times, and the bubble radius evolution for case 1. The time at which a parcel is initially shocked varies as $R^{5/2}$ or $M^{5/6}$. The postshock value of κ varies as M^{-1}, and the corresponding cooling time as $\kappa^{3/2}$. As a consequence, the time at which mass M finishes cooling is

$$t_{cool}(M) = t_1\left(\frac{M}{M_1}\right)^{5/6} + \frac{5}{9}t_1\left(\frac{M_1}{M}\right)^{3/2} \tag{32}$$

where t_1 and M_1 are given in equations (29) and (31). The value of t_{cool} is a minimum at $M = M_1$.

At late times, the first term in (32) is negligible, leading to a simple estimate of the mass still in the hot bubble at time t (that is, with $t_{cool} \geq t$):

$$M_{hot}(t) \approx M_1\left(\frac{5t_1}{9t}\right)^{2/3} \approx \frac{32\ M_\odot}{t_{myr}^{2/3}} \frac{2E_{51}}{n_0^{2/3}} . \tag{33}$$

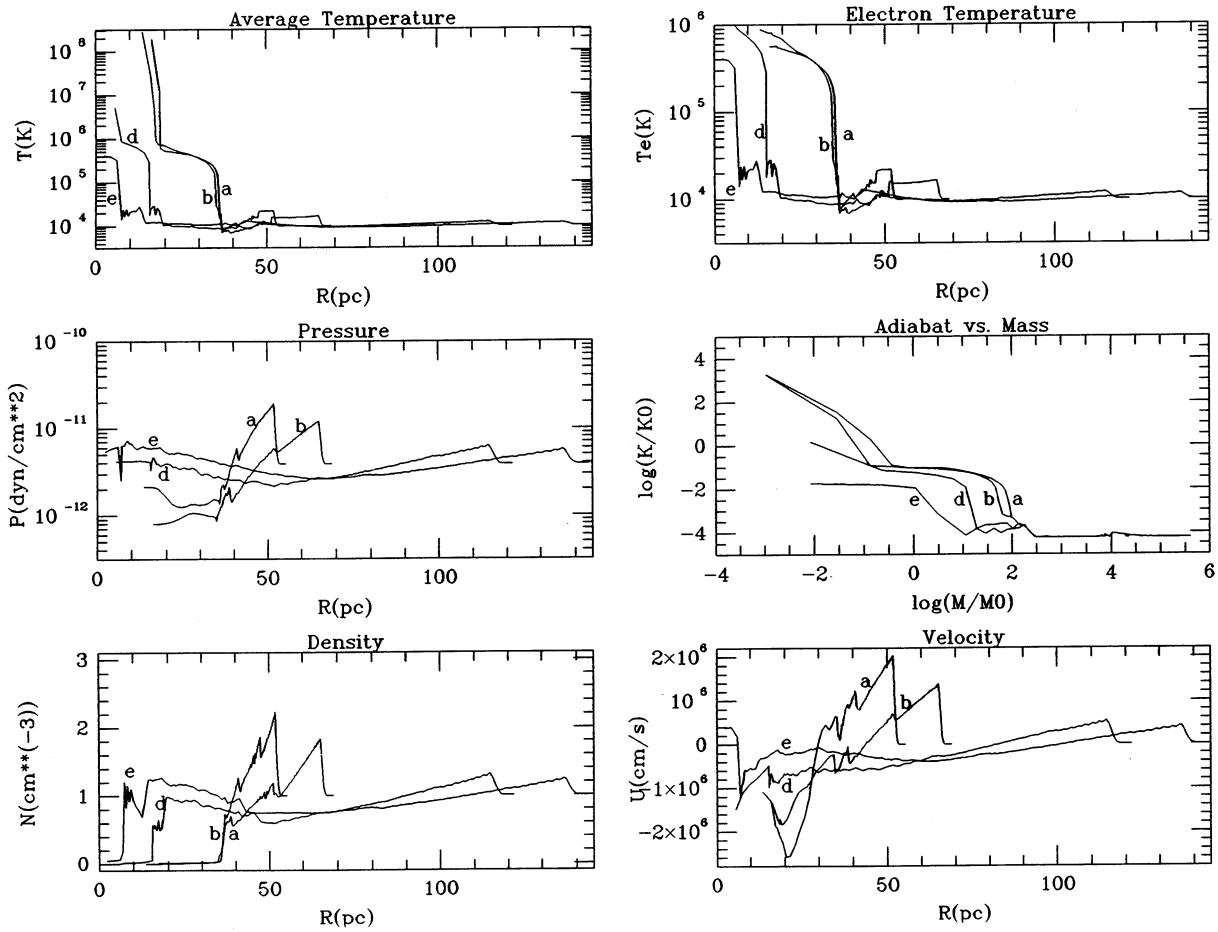

FIG. 6.—Same distributions as those in Fig. 2, but for case 3

In principle, the case 1 results in Figure 10 should agree with this almost exactly. In fact, the numerical result is slightly higher but steeper (30% high at 10^5 yr, 15% high at 10^6 yr, and agreeing well with this result for $t > 2 \times 10^6$ yr). This level of disagreement is negligible considering the modest accuracy we have required. In particular, our initialization scheme resulted in an energy content within the grid about 30% greater than our intended 5×10^{50} ergs. An immediate effect can be seen in Figure 1 where the distribution of adiabats lies about 60% higher for $M > M_0$ (our initialization mass) than its extrapolation from smaller masses where the material is initialized at the Sedov structure. This energy difference is sufficient to understand the excess bubble mass for $t < 2 \times 10^6$ yr. The steeper slope, however, is probably due to a very slight drift in our integration procedure, producing noticeable effects after the enormous number of cycles required to study these late times. In addition, a small part of the steeper slope derives from the criterion used to define the bubble mass when making Figure 10. We included all material hotter than 10^5 K. This fixed criterion forced a very gradually decreasing fraction of the transition region between bubble and shell to be included as the structure evolved.

By assuming that uncooled parcels have essentially their original adiabats, we can use equation (27) to obtain an estimate of the bubble volume at late times. The appropriate value of p is the ambient pressure, the value of κ at the boundary is just that with cooling time equal to t. From equation (23) we find $\kappa^{3/2} = \alpha(\chi k_B)^{1/2} t$ yielding

$$\frac{4}{3}\pi R_B^3 \approx \frac{2.025\pi E_0}{10 p_{\rm center}^{3/5}(4n_0)^{2/3}} \frac{1}{[\alpha(\chi k_B)^{1/2} t]^{4/15}} \tag{34}$$

thus

$$R_B \approx 37.4 \text{ pc} \frac{(2E_{51})^{1/3}}{(10^{12} p_{\rm center})^{1/5} n_0^{2/9} t_{\rm myr}^{4/45}} . \tag{35}$$

As can be seen from Figure 2, the bubble pressure during the collapse varies between $p_0/2$ at early times, and p_0 later, where $p_0 \approx 3.89 \times 10^{-12}$ dyn cm^{-2}. Such overshoot and later recovery is common to explosions. At 1 million yr, $p_{\rm center} = 1.62 \times 10^{-12}$ dyn cm^{-2}, $R_B \approx 34$ pc, dropping to 26 pc at 3 million yr when $p_{\rm center} = 3.4 \times 10^{-12}$ dyn cm^{-2}. Figure 9 shows the numerical results to be 37 and 29 pc, respectively. The 10% discrepancy is due to the inaccuracy of the code, chiefly its consistent assignment of too high adiabats behind the shock, making the results correspond to a somewhat higher energy explosion. Unfortunately, though it would be nice to consider this major flaw in our work, it is dwarfed by several much larger uncertainties, among them the degree of thermal conduction present during the evolution. (For discussion of other uncertainties, see SC.)

5.4. *The Adiabat Distribution for Case 2*

When conduction is present, the distribution of adiabats is altered considerably prior to shell formation, invalidating the

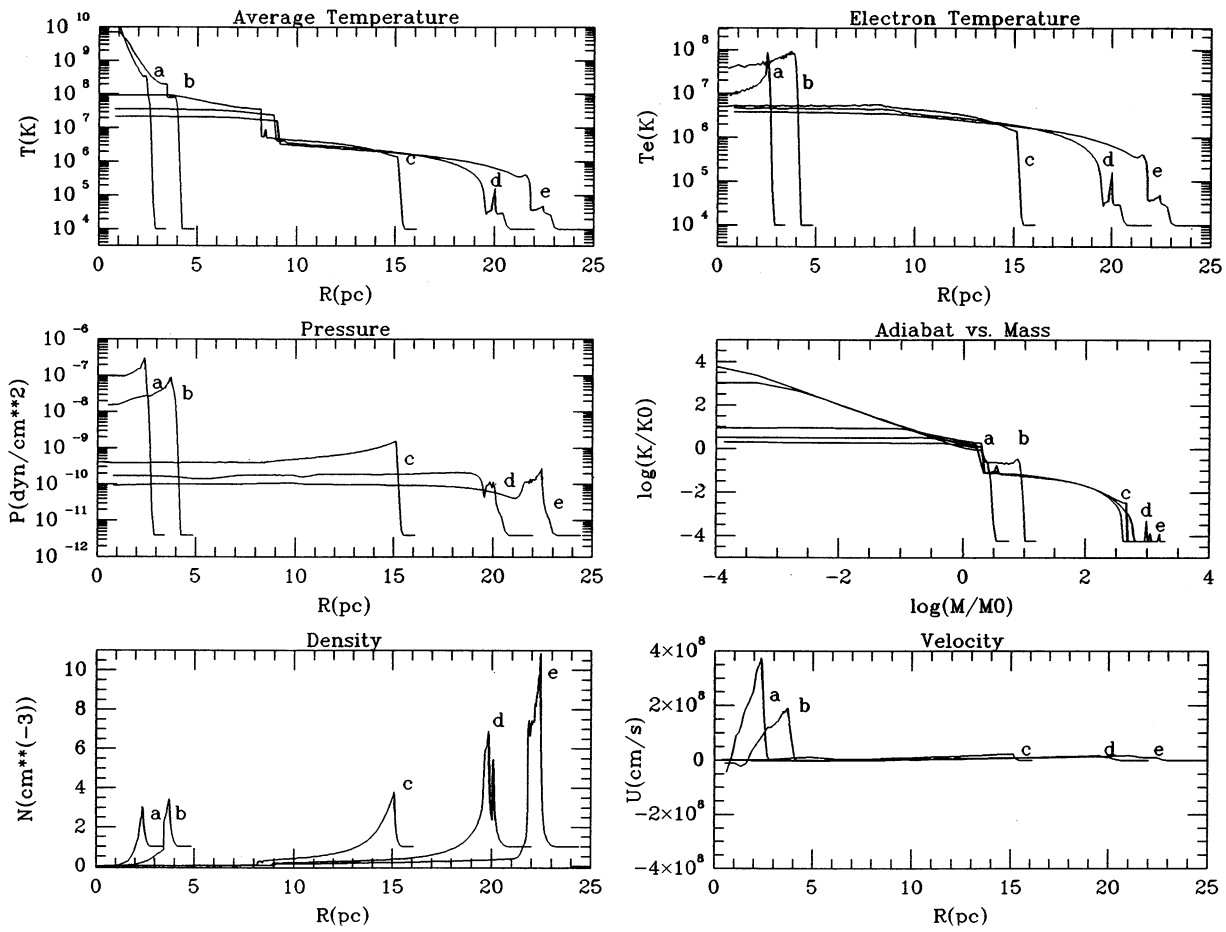

FIG. 7.—Same distributions as those in Fig. 1, but for case 4 (both ion and electron thermal conductions are included, and T_i not equal to T_e).

results of the previous section. The hot mass and bubble size at late times can, however, be estimated if one is able to calculate the adiabat distribution provided by conduction. In this section we present a similarity solution for that distribution which would be approached at late times in the absence of radiative cooling. That solution is a reasonable approximation to the adiabats at the shell-formation epoch, and can be used to infer the bubble mass at later times as cooling eats into it from the outside.

The model yielding the similarity solution starts, at $t = 0$, with all parcels having the values of κ that would be provided by an adiabatic explosion at the origin. In short, shock passage occurs instantaneously through the surroundings, providing the Sedov distribution of adiabats.

In addition, the medium is isobaric, with an evolving pressure function given by that of the central regions of the Sedov solution. Thermal conduction is then released in this environment, to modify the adiabat structure. Saturation of the conduction is ignored. A self-similar structure quickly develops with a characteristic scale $R_c(t)$. Interior to this scale and its associated mass M_c, conduction has flattened the adiabat distribution. In the neighborhood of R_c, the energy conducted from the center produces a shoulder on the adiabat distribution, within which the Sedov values are exceeded. Slightly farther out where the temperature is lower, conduction has so far had little effect.

The solution is derived in the Appendix. A normalized adiabat distribution as a function of the normalized mass is assumed:

$$\kappa/\kappa_c = f(\eta) \quad \text{where} \quad \eta = M/M_c \,. \tag{36}$$

The characteristic values were chosen such that $\kappa \to \kappa_c$ as $M/M_c \to 0$, at the center, and to place M_c within the transition region. For large M, $\kappa M \to (\kappa M)_{\rm Sedov}$ as provided by equation (25). Numerical integration of the structure shows

$$\kappa_c M_c \approx 12(\kappa M)_{\rm Sedov} \,, \tag{37}$$

while the differential equation for the temporal behavior provides

$$\kappa_c^{-71/30} = B(t^{1/25} - t_0^{1/25}) \,. \tag{38}$$

The combination of these two, with time expressed in cgs units, yields

$$\kappa_c^{-71/30} = 9.6 \times 10^{20} \frac{n_0^{208/255}}{(2E_{51})^{26/75}} (t^{1/25} - t_0^{1/25}) \,. \tag{39}$$

For the pure similarity solution, t_0 is the time at which the development began, starting from the Sedov distribution of adiabats. As an approximation to the SNR bubble conditions, however, the similarity solution only gradually becomes relevant because at early times the shock is far inside the characteristic scale of the problem, turning on conduction as it progresses. In order to test equation (39) and to obtain an

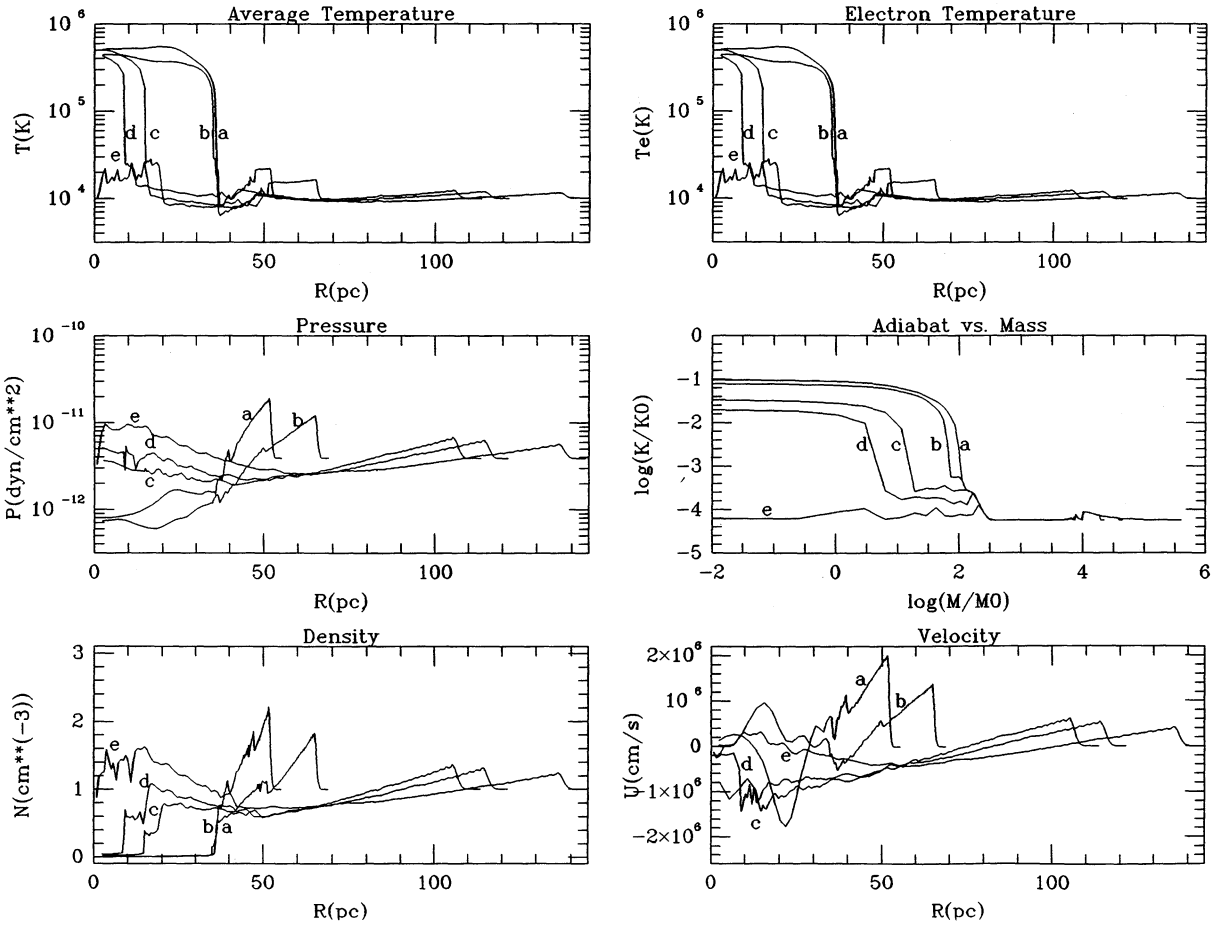

FIG. 8.—Same distributions as those in Fig. 4, but for case 4

estimate of the appropriate delay time t_0, we repeated case 2 with no cooling. The adiabat distribution does approach the similarity structure at late times, and the central adiabat does follow the behavior above, with about the right slope, 1.021×10^{21}. The value of t_0 determined by a fit to these data, and generalized by analogy to equation (6) is

$$t_0 \approx 17{,}000 \text{ yr } (2E_{51})^{3/14} n_0^{-4/7} . \quad (40)$$

We are now prepared to approximate the late evolution of the bubble in case 2.

5.5. *Bubble Mass Evolution with Thermal Conduction*

The principal effect of thermal conduction is to flatten the distribution of adiabats as the remnant approaches shell formation. For $\eta \geq 1.2$, the distribution $f \approx 1/12\eta$ is equivalent to the Sedov solution, but for $\eta \leq 0.7$, the asymptote $f \approx 1 - \eta^{2/3}$

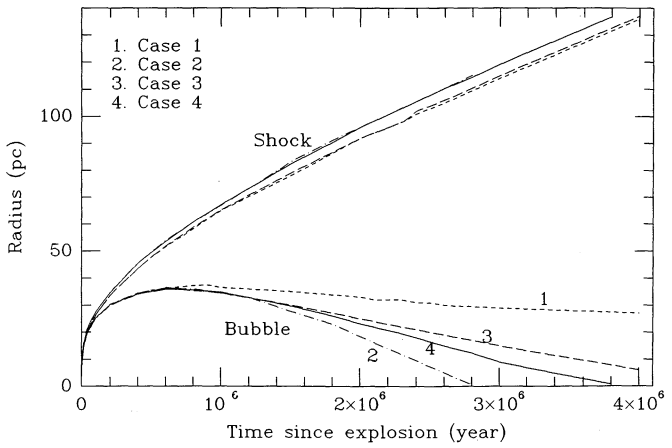

FIG. 9.—Time evolution of the radii of the hot bubble and shock front for cases 1, 2, 3, and 4.

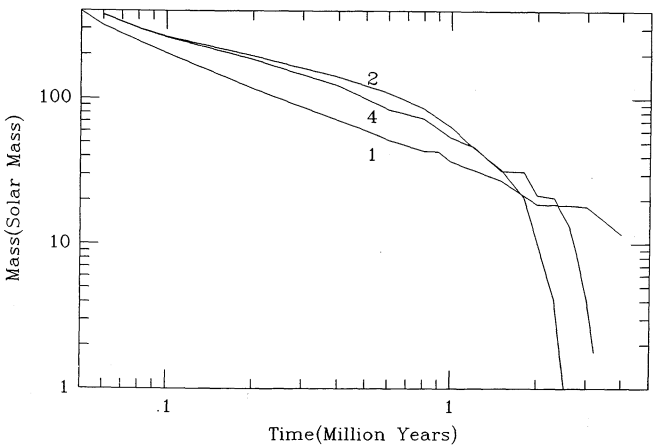

FIG. 10.—Time evolution of mass inside the hot bubble for cases 1, 2, and 4.

is an accurate approximation. (For $\eta = M/M_c$ between 0.7 and 1.2, there is a smooth transition between these two behaviors, joining both from above.) At shell formation, $t \approx 40{,}000$ yr for our cases, equation (39) implies $\kappa_c \approx 4.8 \times 10^{-9}$ cgs, with a corresponding $M_c \approx 135\ M_\odot$. (In deriving these values, we assume $E_0 = 5 \times 10^{50}$ ergs, although our calculations are more representative of a somewhat larger value as discussed previously.)

Applying equation (23),

$$\Delta t_{\rm cool} \approx 4.7 \times 10^6 \text{ yr} \left(\frac{\kappa}{4.8 \times 10^{-9} \text{ cgs}} \right)^{3/2},$$

to the above distributions of $\kappa = f\kappa_c$, the time at which a parcel completes its cooling is $t_{\rm cool}(M) = t_i(M) + \Delta t_{\rm cool}[\kappa(M)]$. Here we have included t_i as the time at which a parcel was initialized to κ (at which the cooling begins). For the Sedov case, $t_i(M)$ is the time at which a parcel was shocked, and was neglected in deriving equation (33). In the presence of thermal conduction, however, we expect some delay in cooling in parcels with $M \approx M_c$ due to the influx of conduction. As a consequence, for the early evolution, we find

$$M_{\rm hot}(t) \approx \frac{32\ M_\odot}{(t_{\rm myr} - \delta)^{2/3}} \tag{41}$$

with β between 0 and 0.04. This delay of cooling is responsible for the roughly 30% difference between case 1 and 2 in Figure 10 for $t < 0.1$ million yr, and from that figure, $\delta \approx 0.02$ at $180\ M_\odot$ appears to be appropriate. With this value, equation (41) should apply for t between roughly 5 to 9×10^4 yr. The latter time asymptote, showing a marked departure from the conduction-free case, is

$$M_{\rm Hot}(t) \approx 135\ M_\odot\ [1 - (t_{\rm myr}/4.7)^{2/3}]^{3/2} \tag{42}$$

and should apply for $t \geq 4 \times 10^5$ yr, $M \leq 100\ M_\odot$.

We have compared these equations with the cooling time versus mass derived from our numerical results for the adiabat distribution at $t = 4 \times 10^4$ yr. The agreement is excellent, overall. It would be perfect if the hot mass were 30% to 40% larger at early times (consistent with an explosion energy that much greater) and κ_c were about 15% smaller, shortening the 4.7×10^6 yr final cooling time to about 3.8×10^6 yr. Both differences are within the limits of our accuracy, and neither disturbs our essential result. Without conduction, equation (41) governs the entire evolution, while with conduction prior to shell formation, equation (42) applies to the last $100\ M_\odot$, bringing the bubble to an abrupt end.

We have not yet considered the effects of thermal conduction after shell formation. By comparing the graph of hot bubble mass versus time calculated from the adiabat distribution at 4×10^4 yr, with the hot bubble mass found in the numerical evolution, we can isolate those effects. We find that prior to 0.7 million yr, there is no difference. After that time, the mass drops more rapidly than projected without conduction, reaching zero at about 2.6 million yr, as seen in Figure 10.

Thus conduction subsequent to shell formation can have a moderate effect on the bubble, shortening its life by 30%. The conduction which matters, however, is that occurring soon after shell formation, and prior to the bubble's reaching maximum size, as we now demonstrate.

Without cooling, the central adiabat would continue to decline, obeying equation (39). The corresponding Kahn cooling time for the center, as a function of time, is therefore

$$t_{\rm cool}(t) = t + \frac{[\kappa_c(t_A)]^{3/2}}{\alpha(\chi k_B)^{1/2}} \left(\frac{t_A^{1/25} - t_0^{1/25}}{t^{1/25} - t_0^{1/25}} \right)^{45/71}. \tag{43}$$

Taking $t_A = 4 \times 10^4$ yr, $[\kappa_c(t_A)]^{3/2}/\alpha(\chi k_B)^{1/2} \approx 4 \times 10^6$ yr, and $t_0 = 1.7 \times 10^4$ yr, we have

$$t_{\rm cool}(t) \approx t + 4 \times 10^6 \text{ yr} \left(\frac{0.052}{t_{\rm yr}^{1/25} - 1.476} \right)^{45/71}. \tag{44}$$

The right term drops rapidly when t is close to t_0, but soon becomes nearly constant while the left term, t, rises. The actual cooling time of the central parcel is approximately the minimum of this function, 2.1×10^6 yr. It minimizes at $t = 4 \times 10^5$ yr when cooling becomes more important than conduction to the subsequent evolution of κ_c.

The procedure above leads to a cooling time estimate of 2.1×10^6 yr, compared with our numerical result of 2.6×10^6 yr. In fact, $t_{\rm cool}$ reaches the latter at $t = 1 \times 10^5$ yr, leading us to believe that conduction is further quenched by the presence of radiative cooling.

6. SUMMARY AND CONCLUSIONS

We modeled the more-or-less standard theorist's remnant, for the first time including separated ion and electron temperatures and their corresponding thermal conductivities, comparing the results with simpler examples. We included a useful approximation to the cooling function, making it possible to develop analytic descriptions of several facets of the behavior. We verified that the code worked well, with two identifiable flaws: it evolved as a slightly more energetic explosion than we attempted to initialize, and after a very long time there was a slight downward drift in the adiabats compared to analytic results.

We verified that a remnant with thermal conduction can be reasonably well modeled with a single temperature if one is primarily concerned with the late-time behavior. Ion conduction is sufficient to eliminate the hot ion zone so that the two-temperature model of case 4 approaches the single-temperature case 2. As a consequence, we confirm that the conclusions of Slavin & Cox (1992) based on models like that of case 2 (but with realistic cooling) are not in jeopardy. In particular, conduction prior to the bubble's reaching its maximum size (mostly prior to shell formation) has an enormous impact on the bubble evolution, but later conduction does not. The bubbles are much smaller and shorter lived than earlier analytic estimates (e.g., McKee & Ostriker 1977), and the so-called dense shells actually reexpand to rejoin the ambient medium. (This occurs partly via the magnetic pressure and partly via an assumed diffuse heating mechanism that prevents the temperature from dropping below 10^4 K. See Slavin & Cox 1992, for further discussions. Aspherical behaviors due to the magnetic forces are also being explored and will be reported elsewhere.)

We found that the details of our case 4 evolution depend somewhat on assumptions made about the ion thermal conductivity and its saturated flux. Detailed investigation on this subject is outside the scope of this paper. (It could be important in young remnants.)

We made significant progress toward the development of analytical approximations to bubble mass and sizes that may be useful in exploring the porosity expected in the interstellar medium as a function of assumed conditions.

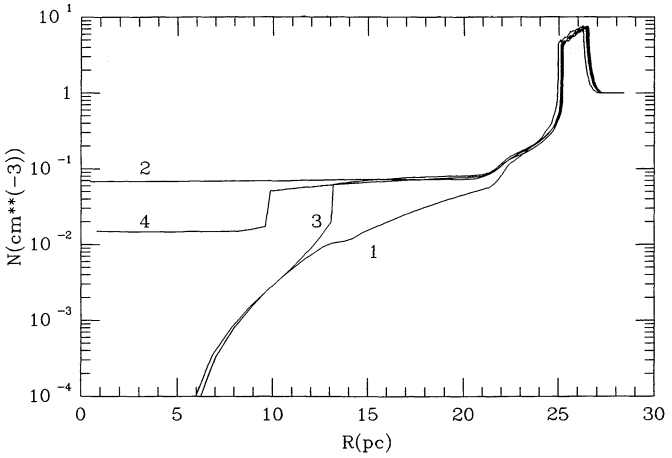

FIG. 11*a*

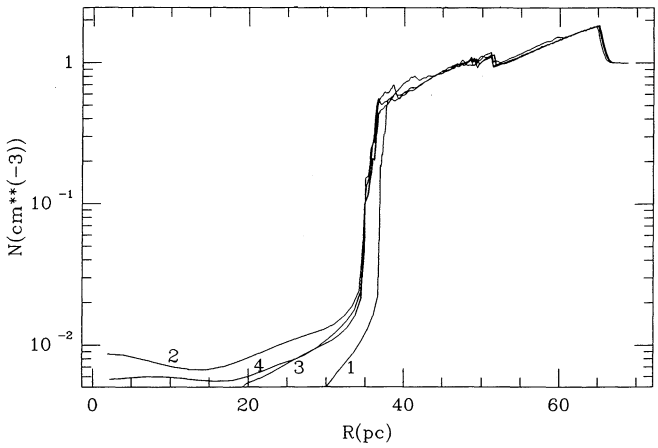

FIG. 11*b*

FIG. 11.—Density distributions at (*a*) 10^5 yr and (*b*) 10^6 yr for cases 1, 2, 3, and 4

We would like to close by introducing Figure 11 which shows rather strikingly the major differences between our four cases. The density distributions for all four are shown at ages of 10^5 and 10^6 yr. The conduction-free case 1 has a very hot very tenuous core within its bubble, the central parts of which are too diffuse to cool on an interesting time scale. At 10^5 yr, the single-temperature conductive case 2 is at the opposite extreme, with an extremely shallow density profile over most of the bubble volume. Cases 3 and 4 resemble case 2 outside of their unequilibrated zone. Case 3 is very similar to 1 in its hot ion core, because its ions are conduction-free. Case 4, on the other hand has a nearly isothermal (flat density) hot in core, with a density jump at the electron-ion equilibration boundary. (This boundary is preserved here by our assumed low value for saturated ion conduction.) Outside the bubble, conduction has had no significant effect.

At $t = 10^6$ yr, after the bubble has reached its maximum size, Figure 11*b* shows a bubble radius of 34 pc, the disappearance of any significant difference between cases 2 and 4 (or case 3 outside its hot ion core), and expansion to central density somewhat below 10^{-2} cm^{-3} for the conductive cases. The density within the nonconductive examples plunges below 10^{-5} cm^{-3} for $R < 12$ to 15 pc. The densities are so low and temperatures so great that it is almost inconceivable that some form of transport would not be active, even in the presence of a potentially tangled magnetic field distribution.

We would like to acknowledge useful discussions with Jon Slavin and Dick Edgar, and Cui would also like to thank Professor Dan McCammon for his encouragement. This research was supported by the National Aeronautics and Space Administration under grants NAGW-2532 and NAG 5-629.

APPENDIX

Summarizing the equations involved, we have

$$\text{Heat flux: } F = -4\pi R^2(\beta T^{5/2})\frac{\partial T}{\partial R} \tag{A1}$$

$$\text{Adiabatic constant: } \kappa = \frac{p}{n^{5/3}} \tag{A2}$$

$$\text{Pressure: } p = p_I(t),\ \frac{dp}{dt} = -\frac{5}{6}\frac{p}{t} \tag{A3}$$

$$\text{Equation of state: } p = \chi n k_B T,\ \chi \equiv \frac{n + n_e}{n} \tag{A4}$$

$$\text{Density: } n = \frac{dN}{dV} \tag{A5}$$

where N is the total number of particles enclosed by the parcel, and V is the enclosed volume, $(4\pi/3)R^3$.

Considering κ and p as the primary variables, combining all the results above, we get

$$F = -\left[\frac{36\pi}{5}\left(\frac{3}{4\pi}\right)^{1/3}\frac{\beta}{(\chi k_B)^{7/2}}\right]p^2\kappa^{1/2}V^{4/3}\frac{\partial \kappa}{\partial N}. \tag{A6}$$

Applying the first law of thermodynamics, we have

$$\frac{1}{\kappa}\frac{D\kappa}{Dt} = -\frac{2}{3}\frac{1}{p}\frac{\partial F}{\partial V} = -\frac{2}{3p}\frac{\partial N}{\partial V}\frac{\partial F}{\partial N}, \tag{A7}$$

where

$$\frac{D}{Dt} = \frac{\partial}{\partial t}\bigg|_{\text{constant } N},$$

therefore

$$\frac{1}{\kappa}\frac{D\kappa}{Dt} = \left[\frac{24\pi}{5}\left(\frac{3}{4\pi}\right)^{1/3}\frac{\beta}{(\chi k_B)^{7/2}}\right]\frac{p^{8/5}}{\kappa^{3/5}}\frac{\partial}{\partial N}\left[V^{4/3}\frac{\partial}{\partial N}\left(\frac{2}{3}\kappa^{3/2}\right)\right]. \tag{A8}$$

Assuming similarity solution

$$\kappa = \kappa_c(N_c) f\left(\frac{N}{N_c}\right), \quad N_c = N_c(t), \tag{A9}$$

and also $\kappa_c \propto 1/N_c$, then we have

$$-\left(1 + \frac{\eta}{f}\frac{df}{d\eta}\right)\frac{1}{N_c}\frac{dN_c}{dt} = \left[\frac{16\pi}{5}\left(\frac{3}{4\pi}\right)^{1/3}\frac{\beta}{(\chi k_B)^{7/2}}\right]\left(\frac{p^{4/5}}{N_c^{2/3}}\kappa_c^{17/10}\right)\frac{1}{f^{3/5}}\frac{\partial}{\partial\eta}\left(g^{4/3}\frac{\partial}{\partial\eta}f^{3/2}\right), \tag{A10}$$

where $\eta = N/N_c$ is the normalized mass, and $g = \int_0^\eta f^{3/5}(\eta)\, d\eta$ is the normalized volume.

We choose N_c and κ_c so that

$$\frac{1}{N_c}\frac{dN_c}{dt} = \left[\frac{16\pi}{5}\left(\frac{3}{4\pi}\right)^{1/3}\frac{\beta}{(\chi k_B)^{7/2}}\right]\left(\frac{p^{4/5}}{N_c^{2/3}}\kappa_c^{17/10}\right). \tag{A11}$$

With $\kappa_c \propto 1/N_c$, we find

$$N_c^{71/30}\frac{1}{N_c}\frac{dN_c}{dt} \propto p^{4/5} \propto (t^{-6/5})^{4/5}, \tag{A12}$$

since $p \propto 1/R^3 \propto 1/t^{6/5}$. Therefore

$$N_c^{71/30} = A(t^{1/25} - t_0^{1/25}), \tag{A13}$$

or equivalently,

$$\kappa_c^{-71/30} = B(t^{1/25} - t_0^{1/25}). \tag{A14}$$

The general differential equation for adiabatic constant, κ, as a function of mass enclosed, is then

$$-\left(1 + \frac{\eta}{f}\frac{df}{d\eta}\right) = \frac{1}{f^{3/5}}\frac{\partial}{\partial\eta}\left(g^{4/3}\frac{\partial}{\partial\eta}f^{3/2}\right) \tag{A15}$$

The asymptotic behaviors are such that at large $\eta, f\eta \to$ constant, i.e., Sedov result, as desired, while at small $\eta, f \to 1 - \eta^{2/3}$, where the value at $\eta = 0$ has been taken to be 1. Thus κ_c corresponds to the value of κ at the center, while N_c is the enclosed particle number where $\eta = 1$.

Numerical integration of equation (A15) establishes that

$$\kappa_c N_c \approx 12(\kappa N)_{\text{Sedov}}, \tag{A16}$$

this allows us to calculate the slope B in equation (A14) above. With time expressed in years and κ in cgs units, we have

$$\kappa_c^{-71/30} = 9.6 \times 10^{20}\frac{n_0^{208/255}}{(2E_{51})^{26/75}}(t^{1/25} - t_0^{1/25}). \tag{A17}$$

REFERENCES

Braginskii, S. I. 1958, Soviet Phys. JETP Lett., 6, 358
Chevalier, R. A. 1975, ApJ, 198, 355
Cioffi, D. F., McKee, C. F., & Bertschinger, E. 1988, ApJ, 334, 252
Cox, D. P. 1972, ApJ, 178, 143
Cox, D. P., & Anderson, P. R. 1982, ApJ, 253, 268
Cox, D. P., & Edgar, R. J. 1983, ApJ, 265, 443
Cox, D. P., & Slavin, J. D. 1992, in preparation
Cox, D. P., & Smith, B. W. 1974, ApJ, 189, L105
Cowie, L. L. 1977, ApJ, 215, 226
Cowie, L. L., & McKee, C. F. 1977, ApJ, 211, 135
Edgar, R. J., & Cox, D. P. 1984, ApJ, 283, 833
Itoh, H. 1978, PASJ, 30, 489
———. 1979, PASJ, 31, 541
Kahn, F. D. 1975, Proc. 15th Internat. Cosmic Ray Conf. (Munich), 11, 3566
———. 1976, A&A, 50, 145
McKee, C. F., & Ostriker, J. P. 1977, ApJ, 218, 148
Raymond, J. C., Cox, D. P., & Smith, B. W. 1976, ApJ, 204, 290
Shklovskii, I. 1973, Soviet Astron.–AJ, 16, 749
Slavin, J. D. 1990, Ph.D. thesis, Univ. Wisconsin-Madison
Slavin, J. D., & Cox, D. P. 1992, ApJ, 392, 131 (SC)
Solinger, A., Rappaport, S., & Buff, J. 1975, ApJ, 201, 381
Spitzer, L. 1962, Physics of Fully Ionized Gases (NY: Interscience)